A novel bias compensation recursive least square-multiple weighted dual extended Kalman filtering method for accurate state-of-charge and state-of-health co-estimation of lithium-ion batteries.

QIAO, J., WANG, S., YU, C., SHI, W. and FERNANDEZ, C.

2021

A novel bias compensation recursive least square-multiple weighted dual extended Kalman filtering method for accurate state-of-charge and state-of-health co-estimation of lithium-ion batteries

Jialu Qiao[1] **Shunli Wang**[1] **Chunmei Yu**[1] **Weihao Shi**[1] **Carlos Fernandez**[2]

[1] School of Information Engineering, Southwest University of Science and Technology, Mianyang, China

[2]School of Pharmacy and Life Sciences, Robert Gordon University, Aberdeen, UK

Correspondence
Shunli Wang, School of Information Engineering, Southwest University of Science and Technology, Mianyang 621010, China. Email: 497420789@qq.com

Abstract

State-of-charge and state-of-health of power lithium-ion batteries are two important state parameters for battery management system monitoring. To accurately estimate the state-of-charge and state-of-health of in real time, the ternary lithium-ion battery is taken as the research object, and a novel bias compensation recursive least square-multiple weighted dual extended Kalman filtering method is proposed innovatively. The noise variance estimation is introduced to compensate the parameters identified by the general least square method to realize the accurate identification. The estimation value is corrected by using the residual and Kalman gain at multiple times, and different weights are configured for each residual according to the amount of information contained. The data of different complex conditions are used to verify the feasi-bility of the proposed algorithm, the results show that the root-mean-square error of bias compensation recursive least square-multiple weighted dual extended Kalman filtering under dynamic stress test and Beijing bus dynamic stress test condition can be controlled within 1.62% and 2.70% in state-of-charge estimation, 0.17% and 0.81% in state-of-health estimation, which verifies that the proposed algorithm in this research has good running effect. The novel bias compensation recursive least square-multiple weighted dual extended Kalman filtering method lays a theoretical foundation for the safe operation of electric vehicles.

KEYWORDS

bias compensation recursive least square, lithium-ion battery, multiple weighted dual extended Kalman filtering, state-of-charge, state-of-health

1 INTRODUCTION

With the rapid development of the industrial level in various countries, the development of clean and renewable energy has become a global issue due to the increasing shortage of resources and environmental pollution.[1–3] In the process of the development of the automobile industry, pure electric vehicles have gradually become the main direction of the development of new energy vehicles because of their low noise,[4] low pollution, simple structure, easy maintenance,

and other advantages.[5] The lithium-ion battery has become the best choice of electric vehicle power source and has been widely applied on account of its large energy density, lightweight, no memory effect, stable charge, and discharge voltage.[6–8] State-of-charge (SOC) and state-of-health (SOH) are two extremely important state parameters of battery management system (BMS).[9] High precision SOC estimation can effectively avoid battery overcharge and overdischarge,[10] protect battery safety, and prolong service life.[11] With the increase of battery charge and discharge times, SOH will gradually decay until the end of life.[12] The performance of aging batteries is seriously degraded, and it is easy to cause a variety of safety problems.[13–15] Therefore, real-time and effective monitoring of SOC and SOH status of power lithium-ion batteries is of great significance to the safety, reliability, and power performance of electric vehicles.

The commonly used SOC and SOH estimation algorithms at home and abroad include direct measurement method, data-driven method, and model-based method.[16,17] Direct measurement is an open-loop estimation method, which usually includes the open-circuit voltage (OCV) method and Ampere-hour.[18,19] In the OCV method, the OCV–SOC relationship is greatly affected by the working environment, and the OCV is the voltage of the battery in the steady state,[20] which will take a lot of time to put the battery from the working state to the equilibrium state.[21] Ampere-hour is widely used method for estimation of SOC, and it has simple calculation and easy implementation.[22] However, it requires high accuracy of initial value, and the error of estimation will be larger and larger with the accumulation of time.[23] The essence of data-driven method is also a kind of open-loop estimation method,[24,25] which is developed with machine learning and artificial intelligence algorithm.[26] But it needs a large amount of data and a high cost of calculation.[27] The model-based method simulates the internal dynamic reaction process of lithium-ion battery by establishing equivalent circuit model,[28] and the parameters of lithium-ion battery in real-time are taken as the input of the equivalent circuit model, and then the SOC is estimated by combining with the filtering algorithm in the control theory.[29]

Xiong et al. use the Kalman filter (KF) algorithm to calculate SOC, which lays the foundation for the next research,[30] but it cannot be applied to nonlinear systems because the state transition matrix A, and calculation measurement matrix C in KF equation are linear. Extended KF (EKF) is proposed to estimate the SOC of the second-order battery model, which makes the algorithm keep high estimation precision under the circumstance of unknown noise and is suitable for nonlinear systems.[31] In Zhi et al.,[32] an extended KF-adaptive unscented KF (EKF-AUKF) algorithm is proposed creatively to estimate SOC of first-order RC battery and higher precision is obtained. An online SOH estimation method based on dual unscented KF (DUKF) algorithm is proposed.[11] Two independent unscented KFs (UKFs) were used to estimate battery SOC and internal resistance at the same time, and the estimation accuracy was higher than that of single UKF algorithm.

To better characterize the battery characteristics and estimate the battery state accurately, in this research, the second-order Resistor-Capacitance (RC) equivalent circuit model is constructed, the bias compensation recursive least square (BCRLS) algorithm which introduces noise variance to compensate the battery parameters is proposed innovatively to identify the parameters online precisely, SOC and SOH is co-estimated by the proposed novel multiple weighted dual extended Kalman filtering (MWDEKF) method.

2 MATHEMATICAL ANALYSIS

The internal dynamic characteristics of lithium-ion batteries mainly depend on their chemical parameters, which cannot be measured by external instruments. Therefore, it is particularly essential to establish a suitable equivalent model for research needs and accurate online parameter identification.

2.1 Second-order RC equivalent circuit modeling

Thevenin model is based on the Rint model, adding an RC circuit to equivalent the internal polarization reaction of the battery, which simply distinguishes the dynamic and static characteristics, but ignores the different speeds of electrochemical polarization reaction and concentration polarization reaction. It is usually solved by adding a certain number of RC circuits. According to the above analysis, an RC circuit is added to the Thevenin model, which can characterize the charge–discharge characteristics of the battery precisely, and the calculation work is not heavy. Accurate modeling and simple calculation are considered comprehensively; the second-order RC equivalent circuit model is built, which is shown in Figure 1.

In Figure 1, the OCV is represented by U_{OC}, the terminal voltage is represented by U_L, the ohmic internal resistance is represented by R_0, where R_1 and R_2 represent the electrochemical polarization resistance and concentration polarization resistance, C_1 and C_2 represent the electrochemical polarization capacitance and concentration polarization capacitance, respectively, and the current I is in the positive direction when discharging. Due to the consideration of Kirchhoff's law, the expressions of voltage and current of the equivalent circuit can be obtained by analyzing the second-order RC equivalent circuit model as shown in Equation 1.

$$U_L = U_{OC} - I(t)R_0 - U_1 - U_2$$

$$\begin{cases} \dfrac{dU_1}{dt} = -\dfrac{U_1}{R_1C_1} + \dfrac{I}{C_1} \\ \dfrac{dU_2}{dt} = -\dfrac{U_2}{R_2C_2} + \dfrac{I}{C_2} \end{cases} \tag{1}$$

where, $[\mathrm{SOC\ U_1\ U_2}]^{\mathrm{T}}$ is selected as the state variable.

2.2 Parameter identification based on BCRLS

Recursive least square (RLS) is an algorithm for parameter identification of model and data mining based on adaptive filtering theory. This method can be applied to the situation that the system model and parameters are greatly affected by external conditions by regularly correcting and updating the system parameters and can capture the real-time characteristics of the system accurately. The discrete equation of the model to be identified and the corresponding difference equation are shown in Equation 2.

$$\begin{cases} G(z) = \dfrac{y(z)}{u(z)} = \dfrac{b_1z^{-1} + b_2z^{-2} + \cdots + b_nz^{-n}}{1 + a_1z^{-1} + a_2z^{-2} + \cdots + a_nz^{-n}} \\ y(k) = -\sum\limits_{i=1}^{n} a_i y(k-i) + \sum\limits_{i=1}^{n} b_i u(k-i) + v(k) \end{cases} \tag{2}$$

where a, b are the parameters to be estimated; y (k) is the k-time observation value of the system output; U (k) is the k-time value of the system input; V (k) is the random noise with the mean value of 0.

In view of the noise signal in the battery measurement data, the traditional RLS cannot identify the battery model parameters with high accuracy, and the accuracy of battery model parameters directly affects the estimation accuracy of battery SOC and SOH. The BCRLS algorithm introduces the noise variance estimation, which can compensate the parameters identified by the general RLS, and realize the accurate identification of the battery model parameters. Parameter initialization of BCRLS is shown in Equation 3.

$$\begin{cases} \widehat{\theta}_c(0) = \theta(0) = \varepsilon \\ J(0) = 0 \\ P(0) = \delta I_0 \end{cases} \tag{3}$$

where $\widehat{\theta}_c(0)$ is the initial value of the bias compensation parameter, $\theta(0)$ is the initial value of the identification parameter by RLS, $J(0)$ is the initial value of error criterion function, and $P(0)$ is the initial value of covariance matrix. δ is generally a large positive number, and I_0 is the identity matrix. The prediction output of the model and estimation error is shown in Equation 4.

$$\begin{cases} \widehat{y}(k) = \phi^T(k)\theta(k-1) \\ e(k) = y(k) - \widehat{y}(k) \end{cases} \tag{4}$$

where $\varphi^T(k) = [-y(k-1), -y(k-2), ..., -y(k-n_a), u(k-1), ..., u(k-n_b)]$, which is a collection of system samples; $\theta(k)$ is parameter vector to be identified. In each iteration, the algorithm uses the difference between the calculated value of the system observation and the actual observation value as well as the gain K to correct the final estimated value. The calculation of gain matrix K and parameter estimation of battery are shown in Equation 5.

$$\begin{cases} K(k) = P(k-1)\phi(k)\left[1 + \phi^T(k)P(k-1)\phi(k)\right]^{-1} \\ \theta(k) = \theta(k-1) + K(k)e(k) \end{cases} \tag{5}$$

The error criterion function $J(k)$ calculation and noise variance $\sigma^2(k)$ estimation are shown in Equation 6.

$$\begin{cases} J(k) = J(k-1) + e^2(k)\left[1 + \phi^T(k)P(k-1)\phi(k)\right]^{-1} \\ \sigma^2(k) = \dfrac{J(k)}{k[1 + \theta_c(k-1)\theta(k-1)]} \end{cases} \tag{6}$$

The update of the covariance matrix $P(k)$ and the parameters $\theta_c(k)$ of the battery model after bias compensation are shown in Equation 7.

$$\begin{cases} P(k) = \left[I - K(k)\phi^T(k)\right]P(k-1) \\ \theta_c(k) = \theta(k) + k\sigma^2(k)P(k)\theta_c(k-1) \end{cases} \tag{7}$$

The battery model is transformed into the least square mathematical form as shown in Equation 8.

$$U_{OC} = U_L + \left(\frac{R_1}{R_1C_1s + 1} + \frac{R_2}{R_2C_2s + 1} + R_0\right)I \tag{8}$$

Let the time constant $\tau_1 = R_1C_1$, $\tau_2 = R_2C_2$, and $a = \tau_1\tau_2$, $b = \tau_1 + \tau_2$, $c = R_0 + R_1 + R_2$, $d = R_1\tau_2 + R_2\tau_1 + R_0(\tau_1 + \tau_2)$. $s = [x(k) - x(k-1)]/T$ is substituted into Equation 8 for discretization, where T means the sampling time, which is shown in the first part of Equation 9. The parameters are abstracted as shown in the second part of Equation 9.

$$\begin{cases} U_{OC}(k) - U_L(k) = \dfrac{-bT - 2a}{T^2 + bT + a}[U_L(k-1) - U_{OC}(k-1)] + \dfrac{a}{T^2 + bT + a}[U_L(k-2) - U_{OC}(k-2)] \\ \qquad + \dfrac{cT^2 + dT + aR_0}{T^2 + bT + a}I(k) + \dfrac{-dT - 2aR_0}{T^2 + bT + a}I(k-1) + \dfrac{aR_0}{T^2 + bT + a}I(k-2) \\ U_{OC}(k) - U_L(k) = k_1[U_L(k-1) - U_{OC}(k-1)] + k_2[U_L(k-2) - U_{OC}(k-2)] \\ \qquad + k_3I(k) + k_4I(k-1) + k_5I(k-2) \end{cases} \tag{9}$$

The identification parameter vector is $\theta = (k_1, k_2, k_3, k_4, k_5)^T$. Let $k_1 = (-bT-2a)/(T^2+bT+a)$, $k_2 = a/(T^2+bT+a)$, $k_3 = (cT^2+dT+aR_0)/(T^2+bT+a)$, $k_4 = (-dT-2aR_0)/(T^2+bT+a)$, $k_5 = aR_0/(T^2+bT+a)$. After the identification, the actual parameters are obtained by Equation 10.

$$\begin{cases} R_0 = \dfrac{k_5}{k_2} \\ R_1 = (\tau_1 c + \tau_2 R_0 - d)/(\tau_1 - \tau_2) \\ R_2 = c - R_1 - R_0 \\ C_1 = \tau_1/R_1, C_2 = \tau_2/R_2 \end{cases} \tag{10}$$

2.3 Multiple weighted calculation

EKF algorithm transforms nonlinear problems into linear ones by Taylor expansion of nonlinear systems. However, if the nonlinearity of the system is very strong, using the EKF algorithm directly will violate the assumption of local linear approximation. With the iteration of the algorithm, it is easy to cause the accumulation of errors. To improve the adaptability of EKF in a nonlinear system, the scalar innovation is extended to innovation matrix, and an innovation-based identification theory and method is established.

Based on the multiple innovation theory, the innovation $e(k) = U_L(k) - C_k x(k|k-1)$ is extended to the innovation matrix $E(p,k)$ as shown in the first part of Equation 11. To adapt to the compatibility of calculation, the extended KF gain $K(k)$ is extended to the filter gain matrix $K(p,k)$ as shown in the second part of Equation 11.

$$\begin{cases} E(p,k) = [e(k)\ e(k-1)\ \cdots\ e(k-p+1)]^T \\ K(p,k) = [K(k)K(k-1)\cdots\ K(k-p+1)] \end{cases} \tag{11}$$

When the innovation matrix $e(p,k)$ and filter gain matrix $K(p,k)$ are introduced into the standard extended KF algorithm, the state update equation is shown in Equation 12. Where p is the time step.

$$\widehat{x} = \widehat{x}(k|k-1) + K(p,k)E(p,k) \tag{12}$$

Although the multiple-extended Kalman filtering (M-EKF) algorithm introduces the innovation scalar of multiple times to form the innovation matrix $e(p,k)$, which makes the accuracy of M-EKF for nonlinear system, state estimation has been improved compared with EKF, but it is still not accurate enough. Because the innovation $e(k)$ of different times in innovation matrix is different from the current time, it is generally considered that the amount of information contained in it is also different, so we cannot simply treat all innovations as the same. Therefore, different weight factors should be configured as shown in Equation 13.

$$\begin{cases} \beta_1 = 1 \\ \beta_2 = \beta_3 = \cdots \beta_p = \dfrac{a}{p-1} \end{cases} \tag{13}$$

where p is the innovation data width and a is the allocation coefficient which is equal to 1.98. The weighted multiple innovation matrix and state update equation are shown in Equation 14.

$$\begin{cases} \widetilde{E}(p,k) = \left[\beta_1 e(k)\ \beta_2 e(k-1)\ \cdots\ \beta_{k-p+1} e(k-p+1)\right]^T \\ \widehat{x} = \widehat{x}(k|k-1) + K(p,k)\widetilde{E}(p,k) \end{cases} \tag{14}$$

To sum up, the principle of multiple weighted calculation is shown in Figure 2.

2.4 Multiple weighted dual extended Kalman filtering

The capacity of the battery will gradually decrease with the increase of battery life, and the decrease of capacity will lead to the decrease of SOH, so the change of battery capacity can predict the change of SOH. Therefore, capacity is selected as the state variable of SOH estimation, which is shown in Equation 15.

$$SOH_Q = \frac{Q_{now}}{Q_{start}} \tag{15}$$

Dual extended KF (DEKF) algorithm uses two KFs to estimate battery capacity and SOC, respectively. One of the KFs uses EKF to estimate SOC, which takes SOC as the only state variable and battery capacity as a constant. Another KF uses EKF algorithm to estimate the battery capacity, which takes SOC as the input value and battery capacity as the state variable. The change of battery SOH can be obtained by predicting the attenuation of capacity. Therefore, DEKF algorithm can jointly estimate SOC and SOH. In the process of combination, the parameters in the model are updated and calculated by the observed variables to improve the estimation accuracy of the algorithm.

The state equation and system observation equation of DEKF algorithm can be written in the form of Equation 16.

$$\begin{cases} \begin{bmatrix} SOC_{k+1} \\ U_{1,k+1} \\ U_{2,k+1} \end{bmatrix} = \begin{bmatrix} 1 & 0 & 0 \\ 0 & e^{-\Delta t/\tau_1} & 0 \\ 0 & 0 & e^{-\Delta t/\tau_2} \end{bmatrix} \begin{bmatrix} SOC_k \\ U_{1,k} \\ U_{2,k} \end{bmatrix} + \begin{bmatrix} -\dfrac{\Delta t}{Q_k} \\ R_1\left(1-e^{-\Delta t/\tau_1}\right) \\ R_2\left(1-e^{-\Delta t/\tau_2}\right) \end{bmatrix} I_k + w_k \\ Q(k+1) = Q(k) + r(k) \\ U_{L,k+1} = U_{OC,k+1} - U_{1,k+1} - U_{2,k+1} - IR_0 + v_k \end{cases} \tag{16}$$

Since the capacity of the battery will decay with the increase of the number of battery cycles, an external noise R is added to the state equation to estimate the capacity to simulate the attenuation process of the battery capacity. The coefficient matrix of state equation and observation equation are shown in Equation 17, respectively.

$$\begin{cases} A_k^x = \begin{bmatrix} 1 & 0 & 0 \\ 0 & e^{-\Delta t/\tau_1} & 0 \\ 0 & 0 & e^{-\Delta t/\tau_2} \end{bmatrix} \\ B_k^x = \begin{bmatrix} -\dfrac{\Delta t}{Q_k} \\ R_1\left(1-e^{-\Delta t/\tau_1}\right) \\ R_2\left(1-e^{-\Delta t/\tau_2}\right) \end{bmatrix} \\ A_k^Q = 1 \\ C_k^x = \begin{bmatrix} \dfrac{\partial U_{OC}}{\partial SOC} & -1 & -1 \end{bmatrix} \\ C_k^Q = -\dfrac{i\Delta t}{Q^2} \end{cases} \tag{17}$$

Among them, A_k^x, B_k^x, and C_k^x are state equation coefficient matrix and observation equation coefficient matrix for SOC estimation, A_k^Q and C_k^Q are state equation coefficient matrix and observation equation coefficient matrix for battery capacity estimation. $w(k)$ is the process noise of SOC estimation at k, and $r(k)$ is the process noise of capacity estimation at k. $w(k)$ and $r(k)$ are Gaussian white noise with zero mean and w and r variance, respectively. $v(k)$ is the measurement noise with zero mean and v variance. $w(k)$ and $r(k)$ are not related to $v(k)$.

The flow chart of DEKF algorithm using two filters to estimate SOC and capacity is shown in Figure 3.

The BCRLS algorithm for online parameter identification is combined with the multiple weighted algorithm and DEKF algorithm to form a novel BCRLS-multiple weighted dual extended Kalman filtering (BCRLS-MWDEKF) algorithm for joint estimation of battery SOC and SOH.

3 EXPERIMENTAL ANALYSIS

To verify the working effect of the proposed algorithm in this research, the dynamic relationship between each parameter and SOC is obtained through online identification and applied in the algorithm. The experimental verification was carried out under different complex operating conditions such as DST (dynamic stress test), BBDST (Beijing bus dynamic stress test) and the proposed algorithm is compared with other algorithms to get better verification.

3.1 Test platform construction

Experimental data used for algorithm verification need to be obtained through experiments of battery. Lithium-ion aluminum shell cell with rated capacity of 50AH and nominal voltage of 3.7 V produced by Delip Battery Technology Co., Ltd. is used for experiment, BTS200-100-104 battery testing equipment provided by Shenzhen Yakeyuan Technology Co., Ltd. is used as the experimental platform. The lithium-ion battery used in the experiment is shown in Figure 4A, the experimental equipment that can charge and discharge, monitor and record the current and voltage state in real-time is shown in Figure 4B.

3.2 Online parameter identification results

According to the definition of OCV, it can only be measured when the battery gets stabilized. OCV–SOC curve can be obtained by experiment which can be described as follows: The battery is fully charged, then it is discharged to a specific SOC at constant current, and the battery is waited until reaching a stable state. At this time, the OCV value corresponding to this SOC value is measured. The process is repeated by discharging the battery from 0.9 to 0.8 SOC until the battery is discharged to 0 SOC to obtain the discharge OCV–SOC curve. It can be seen from Figure 5A that the OCV is 3.9443 V when SOC is 0.8. To consider the hysteresis effect of the battery, the battery is charged in the same way. Generally, the OCV–SOC curve of charge and discharge is not coincident, but a group of banded hysteresis structures with the gap between the ends will be formed. The OCV–SOC curve obtained in the charging process will be slightly higher than that obtained in the discharge process, which is shown in Figure 5B. *Uoc*1 represents the charge OCV curve, and *Uoc*2 represents the discharge OCV curve. Then the accurate OCV is obtained by averaging.

The hybrid pulse power characterization (HPPC) working condition data at room temperature are selected for online parameter identification of the model. The HPPC experiment steps are as follows:

1. The battery is charged with constant current and constant voltage at a voltage of 4.2 V and a current of 1C until it is fully charged. The basic current is 50 A.
2. The battery is placed for 40 min, then is discharged at 1C constant current for 10 s, and then the battery is placed for 40 s. To recover the power of the battery before discharge, the battery is charged with 1C constant current for 10 s, and then is put aside for 3 min after charging.
3. Step 2 is the whole process of one pulse charge and discharge. After that, the battery is discharge at 1C constant current for 6 min to reduce the capacity by 10%. Steps 2 and 3 are repeated for 10 times.

The BCRLS algorithm is validated by the experimental data obtained from HPPC to obtain the dynamic changes of internal parameters of lithium-ion battery at different times, and the identification results of ohmic resistance R_0, polarization resistance R_1 and R_2, and polarization capacitance C_1 and C_2 at different SOC stages are obtained; the dynamic parameter identification results are shown in Figure 6.

The online parameter identification results are used as the input of the model to get the simulated voltage and then compared with the measured voltage to analyze the accuracy of parameter identification. The experimental results are shown in Figure 7.

In Figure 7A, $U1$ represents the measured voltage value, $U2$ represents the simulation voltage value corresponding to offline identification based on curve fitting, $U3$ represents the simulation voltage value identified by RLS, and $U4$ represents the simulation voltage value identified by BCRLS. In Figure 7B, Err1 $\sim$ Err3 represent the simulation voltage error curve corresponding to $U2 \sim U4$. It can be seen that in each cycle, the simulation error of battery charging and discharging part at the moment of current mutation is relatively large, which is related to the violent chemical reaction inside the lithium-ion battery. The estimation error of BCRLS is controlled within 0.0131, less than 0.311%. The experimental results show that the BCRLS algorithm can obtain high-precision online parameter identification results, which can be used in the subsequent SOC and SOH co-estimation.

3.3 Experimental verification under DST operating condition

To verify the operation effect of SOC and SOH co-estimation of the proposed algorithm for lithium-ion batteries under complex application conditions, the self-defined DST experimental data are used for verification. The battery is charged with 1C rate constant current until the upper limit termination voltage is 4.2 V. After charging, the battery is shelved for 30 min to stabilize the battery voltage. Constant current discharge and constant current charge were carried out at 0.5C rate for 4 min, and then constant current discharge was carried out at 1C rate for 4 min. These three steps are cycled until the end of discharge. The optimal value of innovation data width p should be determined according to many times of debugging, and the estimation effect under different values should be compared. In this case, $p = 4$. The simulation results of RLS-DEKF, BCRLS-DEKF, and BCRLS-MWDEKF under DST operating condition are shown in Figure 8.

According to Figure 8B, in the early stage of discharge, the estimation accuracy of BCRLS-MWDEKF is not too high, compared with the other two algorithms, it does not show obvious advantages. However, in the middle and late stages of discharge, the error of RLS-DEKF changes more smoothly, and the estimation accuracy of BCRLS-DEKF improves significantly, which reflects the huge improvement of parameter identification accuracy by adding bias compensation in the algorithm, thus indirectly improving the SOC estimation accuracy. The convergence of BCRLS-MWDEKF is nice, it can track the real value well and achieve good estimation accuracy, which reflects the promotion of multiple weighted algorithm of the SOC estimation. According to Figure 8D, in the later stage of discharge, the SOH estimation value of the battery fluctuates greatly, resulting in the accumulation of errors, which is related to the strong chemical reaction inside the battery itself. However, in this case, BCRLS-MWDEKF still has a good estimation accuracy, and the maximum error is only 0.31%. The estimated value of BCRLS-DEKF is relatively stable in the early stage, but the error increases in the later stage. RLS-DEKF has a strong divergence and cannot track the real value accurately. By comparing the estimation results of SOC and SOH, it shows the superiority of the proposed BCRLS-MWDEKF algorithm. The estimation results of the three algorithms are compared through the maximum error, mean absolute error (MAE), and root-mean-square error (RMSE) under DST working condition as shown in Table 1.

3.4 Experimental verification under BBDST operating condition

BBDST working condition is obtained from the real data collection of the Beijing bus dynamic stress test, including the data of the bus in the start, taxiing, acceleration, rapid acceleration, and other operations, which is authentic and dynamic. The practical application condition of high-power lithium-ion batteries is complex and changeable. It will be more convincing to use BBDST experimental data to verify the feasibility of the proposed algorithm. In this case, the innovation data width $p = 4$. The simulation results of RLS-DEKF, BCRLS-DEKF, and BCRLS-MWDEKF under BBDST operating condition are shown in Figure 9.

Figure 9B shows the error of SOC estimation, the convergence of RLS-DEKF is poor and the error accumulation phenomenon is obvious, the maximum error is up to 2.44% at the end of discharge. The estimation accuracy of BCRLS-DEKF is higher than that of RLS-DEKF, but it fluctuates sharply in the early stage. BCRLS-MWDEKF has the best performance, and the simulated value always deviates from the real value in the whole process of the experiment. The experimental results in Figure 9D show that the SOH maximum error estimated by the three methods is 2.69%, 2.28%, and 1.89%, respectively. In this complex condition, BCRLS-MWDEKF still has the best accuracy. The estimation results of the three algorithms are compared through the maximum error, MAE, and RMSE under BBDST working condition as shown in Table 2.

Through the comparison of the above experimental results, it can be concluded that the BCRLS-MWDEKF algorithm has good accuracy and performance.

4 CONCLUSIONS

Accurate SOC and SOH estimation of high-power lithium-ion batteries is of great significance to the development of new energy vehicles. In this research, the second-order RC model is applied to characterize the state and characteristics of the battery, and the BCRLS method is applied for online parameter identification. To improve the accuracy of battery state estimation, a novel multiple weighted dual extended Kalman filtering method which can make full use of multiple time information and realize the collaborative estimation of SOC and SOH is proposed. The experimental data of DST and BBDST operating conditions are used for verification based on three different algorithms for comparison. The results show that the RMSE of the novel BCRLS-multiple weighted dual extended Kalman filtering under DST and BBDST condition can be controlled within 1.62% and 2.70% in SOC estimation and 0.17% and 0.81% in SOH estimation; the accuracy and performance are greatly improved. The research has positive significance to improve the accuracy of state estimation of lithium-ion batteries and promote the further development of new energy vehicles.

ACKNOWLEDGMENTS

The work was supported by National Natural Science Foundation of China (No. 61801407).

DATA AVAILABILITY STATEMENT

The data that support the findings of this study are available from the corresponding author upon reasonable request.

REFERENCES

1. Aaldering LJ, Leker J, Song CH. Analysis of technological knowledge stock and prediction of its future development potential: the case of lithium-ion batteries. *J Clean Prod*. 2019;223:301-311.
2. Pourjafar S, Shayeghi H, Sedaghati F, Seyedshenava S, Blaabjerg F. A bidirectional multiport DC–DC converter applied for energy storage system with hybrid energy sources. *Int J Circuit Theory Appl*. 2021;49:1849-2297.
3. Mayer R, El Kattel MB, Jeske E, Oliveira SVG. Efficiency evaluation of a bridgeless totem-pole power factor correction rectifier using GaN and insulated gate bipolar transistor devices for battery charger. *Int J Circuit Theory Appl*. 2021;49(4):1133-1146.
4. Xu PP, Li JQ, Sun C, Yang GD, Sun FC. Adaptive state-of-charge estimation for lithium-ion batteries by considering capacity degradation. *Electronics*. 2021;10(2):122-135.
5. Zhang SZ, Guo X, Zhang XW. Modeling of back-propagation neural network based state-of-charge estimation for lithium-ion batteries with consideration of capacity attenuation. *Adv Electr Comput Eng*. 2019;19:3-10.
6. Yang H, Sun X, An Y, Zhang X, Wei T, Ma Y. Online parameters identification and state of charge estimation for lithium-ion capacitor based on improved Cubature Kalman filter. *J Energy Storage*. 2019;24:11-27.
7. Xu Y, Hu M, Zhou A, et al. State of charge estimation for lithium-ion batteries based on adaptive dual Kalman filter. *Appl Math Model*. 2019;1-15.
8. Yang F, Li W, Li C, Miao Q. State-of-charge estimation of lithium-ion batteries based on gated recurrent neural network. *Energy*. 2019; 175:66-75.
9. Duan W, Song C, Chen Y, et al. Online parameter identification and state of charge estimation of battery based on multitimescale adaptive double Kalman filter algorithm. *Math Probl Eng*. 2020;1-14.
10. Zhang S, Guo X, Zhang X. A novel one-way transmitted co-estimation framework for capacity and state-of-charge of lithium-ion battery based on double adaptive extended Kalman filters. *J Energy Storage*. 2021;33:58-72.

11. Xu YD, Hu M, Zhou A, et al. State of charge estimation for lithium-ion batteries based on adaptive dual Kalman filter. *Appl Math Model*. 2020;77:1255-1272.
12. Feng L, Ding J, Han YY. Improved sliding mode based EKF for the SOC estimation of lithium-ion batteries. *Ionics*. 2020;26(6): 2875-2882.
13. Zhu Q, Chen JX, Xu ME, Zou C. Iterative learning based model identification and state of charge estimation of lithium-ion battery. *IET Power Electron*. 2019;12(4):852-860.
14. Dong G, Chen Z, Wei J. Sequential Monte Carlo filter for state of charge estimation of lithium-ion batteries based on auto regressive exogenous model. *IEEE Trans Ind Electron*. 2019;66(11):8533-8544.
15. Yang K, Zewang C, He Z, Wang Y, Zhaihe Z. Online estimation of state of health for the airborne Li-ion battery using adaptive DEKF-based fuzzy inference system. *Soft Comput*. 2020;24(24):18661-18670.
16. Hu L, Junsan Q. Research on active equalization control method of lithium ion battery pack in charging mode. *Time Car*. 2021;03:87-88.
17. Al Chawa MM, Picos R, Roldan JB, Jimenez-Molinos F, Villena MA, de Benito C. Exploring resistive switching-based memristors in the charge-flux domain: a modeling approach. *Int J Circuit Theory Appl*. 2018;46:29-38.
18. Lai X, Wang SY, Ma SD, Xie JY, Zheng YJ. Parameter sensitivity analysis and simplification of equivalent circuit model for the state of charge of lithium-ion batteries. *Electrochim Acta*. 2020;330:1-13.
19. Shu X, Li G, Shen J, Yan W, Chen Z, Liu Y. An adaptive fusion estimation algorithm for state of charge of lithium-ion batteries considering wide operating temperature and degradation. *Power Sources*. 2020;462:1-15.
20. Xiong W, Mo Y, Yan C. Lithium-ion battery parameters and state of charge joint estimation using bias compensation least squares and the alternate algorithm. *Math Probl*. 2020;2020:1-16.
21. Bo P. Research on battery charging control of China standard EMU. *J Beijing Jiaotong Univ*. 2020;3:96-107.
22. Fang L, Li J, Peng B. Online estimation and error analysis of both SOC and SOH of lithium-ion battery based on DEKF method. *Energy Procedia*. 2019;158:3008-3013.
23. Xie Z. Research and development of high precision parameter detection and SOC estimation equipment for energy storage battery pack. *J Beijing Jiaotong Univ*. 2020;3:88-103.
24. Zhang GD, Chen WC, Yu SMS, Aroudi E. A hourglass-shaped impedance network based nonelectrolytic capacitors high step-up converter with low voltage stress. *Int J Circuit Theory Appl*. 2021;49(4):1147-1163.
25. Xuan D, Shi Z, Chen J, Zhang C, Wang Y. Real-time estimation of state-of-charge in lithium-ion batteries using improved central difference transform method. *J Clean Prod*. 2020;252:1-16.
26. Wang R, Feng H. Lithium-ion batteries remaining useful life prediction using wiener process and unscented particle filter. *J Power Electron*. 2020;20(1):270-278.
27. Zhang S, Guo X, Zhang X. An improved adaptive unscented Kalman filtering for state of charge online estimation of lithium-ion battery. *J Energy Storage*. 2020;32:1-17.
28. Gao S, Kang M, Mingren L. Estimation of state-of-charge based on unscented Kalman particle filter for storage lithium-ion battery. *J Eng Des*. 2019;16:1858-1863.
29. Wang Q, Feng X, Zhang B, Gao T, Yang Y. Power battery state of charge estimation based on extended Kalman filter. *Renew Sustain Energy*. 2019;11:1-15.
30. Liu T, Tang X, Wang H, Yu H, Hu X. Adaptive hierarchical energy management design for a plug-in hybrid electric vehicle. *IEEE Trans Veh Technol*. 2020;68:11513-11522.
31. Afshar S, Morris K, Khajepour A. State-of-charge estimation using an EKF-based adaptive observer. *IEEE Trans Control Syst Technol*. 2019;27(5):1907-1923.
32. Zhi L, Peng Z, Zhifu W, Qiang S, Yinan R. State of charge estimation for Li-ion battery based on extended Kalman filter. *Energy Procedia*. 2017;105:3515-3520.

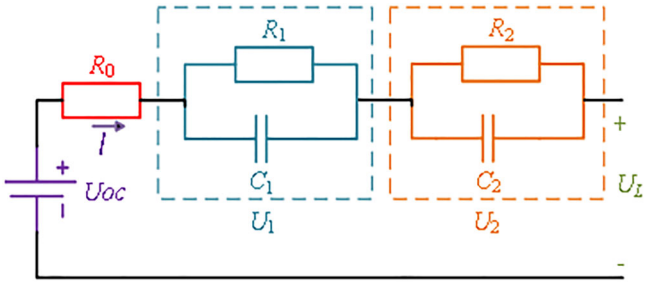

FIGURE 1 Second-order RC equivalent circuit model.

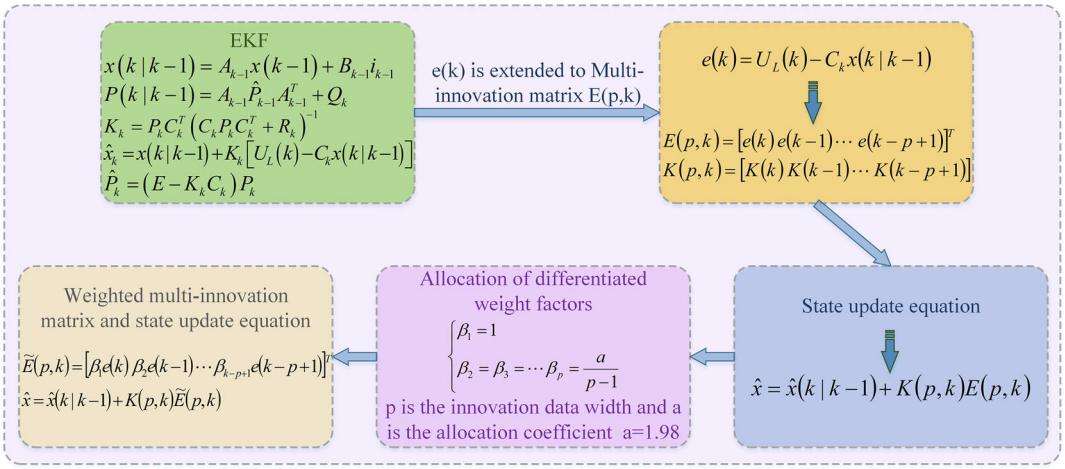

FIGURE 2 The principle of multiple weighted calculation.

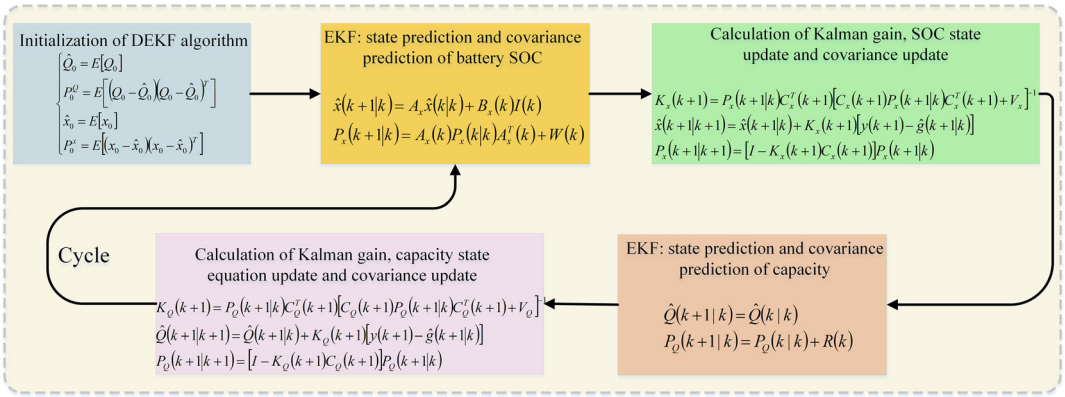

FIGURE 3 The process of SOC and SOH co-estimation by DEKF.

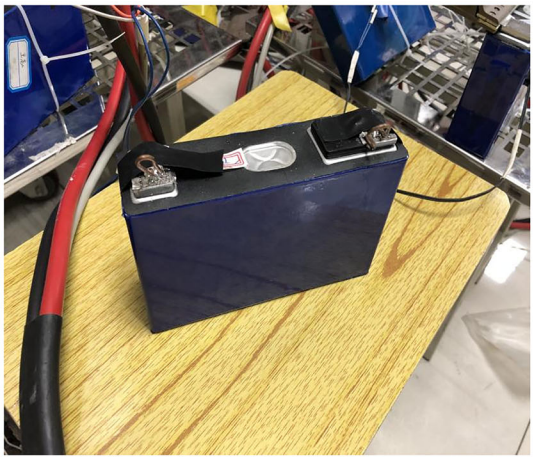

(A)

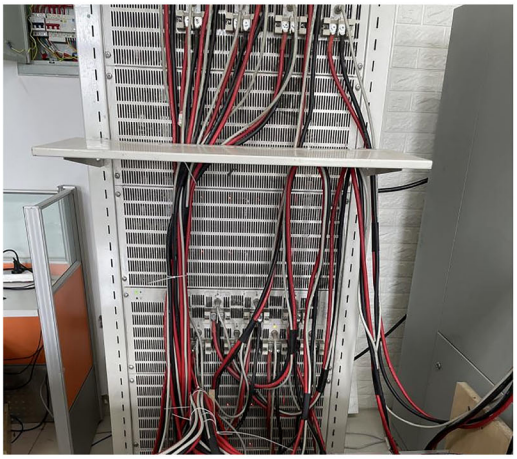

(B)

FIGURE 4 Experimental equipment. (A) Lithium-ion battery used in the experiment. (B) BTS200-100-104 battery testing equipment.

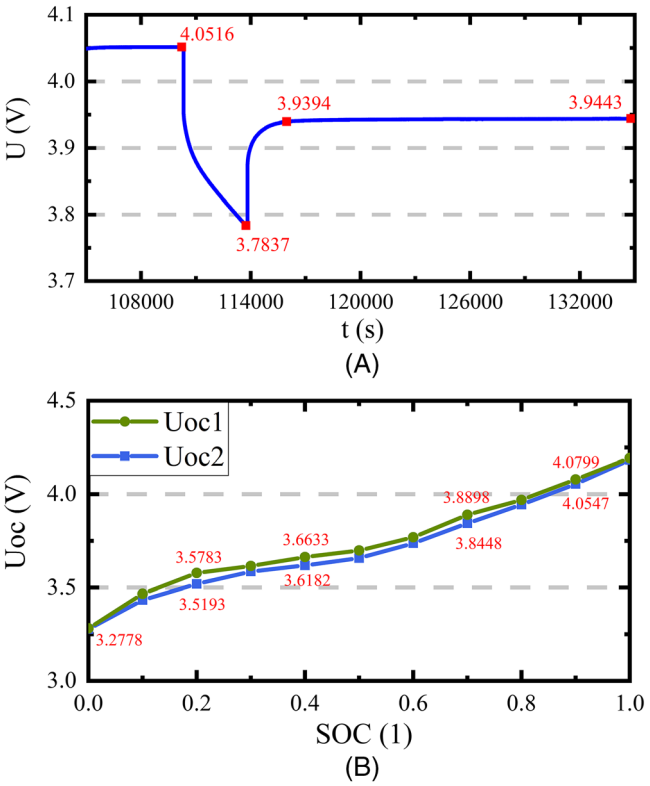

FIGURE 5 Hysteresis characteristic curve of battery OCV. (A) OCV when SOC is 0.8. (B) OCV–SOC curve.

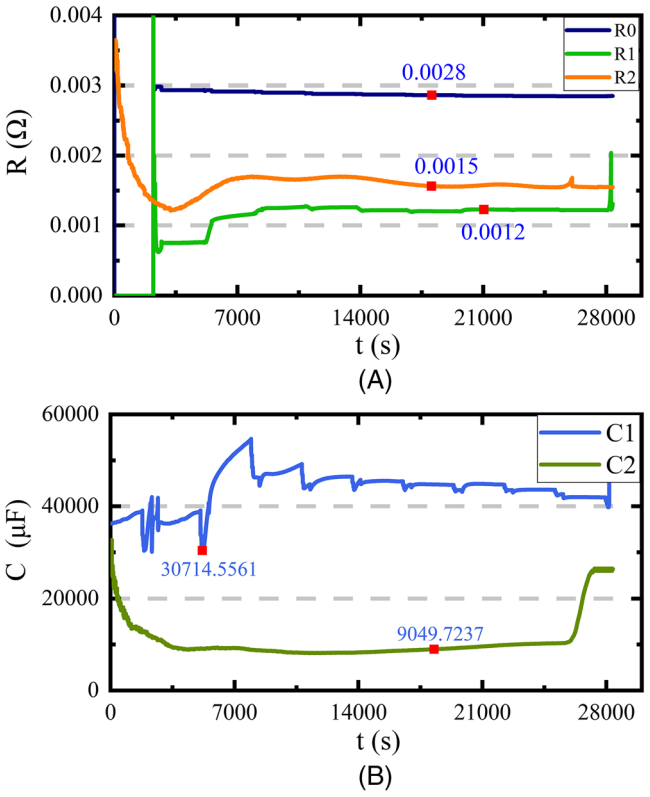

FIGURE 6 Online parameter identification results. (A) Parameter identification results of R_0, R_1, and R_2. (B) Parameter identification results of C_1 and C_2.

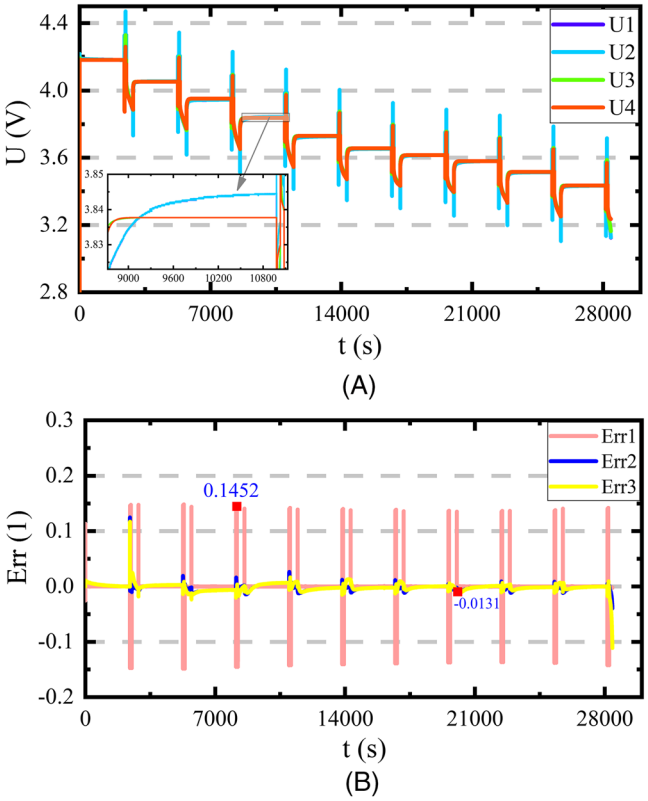

FIGURE 7 Parameter identification results under HPPC working condition. (A) Comparison of parameter identification results under HPPC working condition. (B) Parameter identification error under HPPC working condition

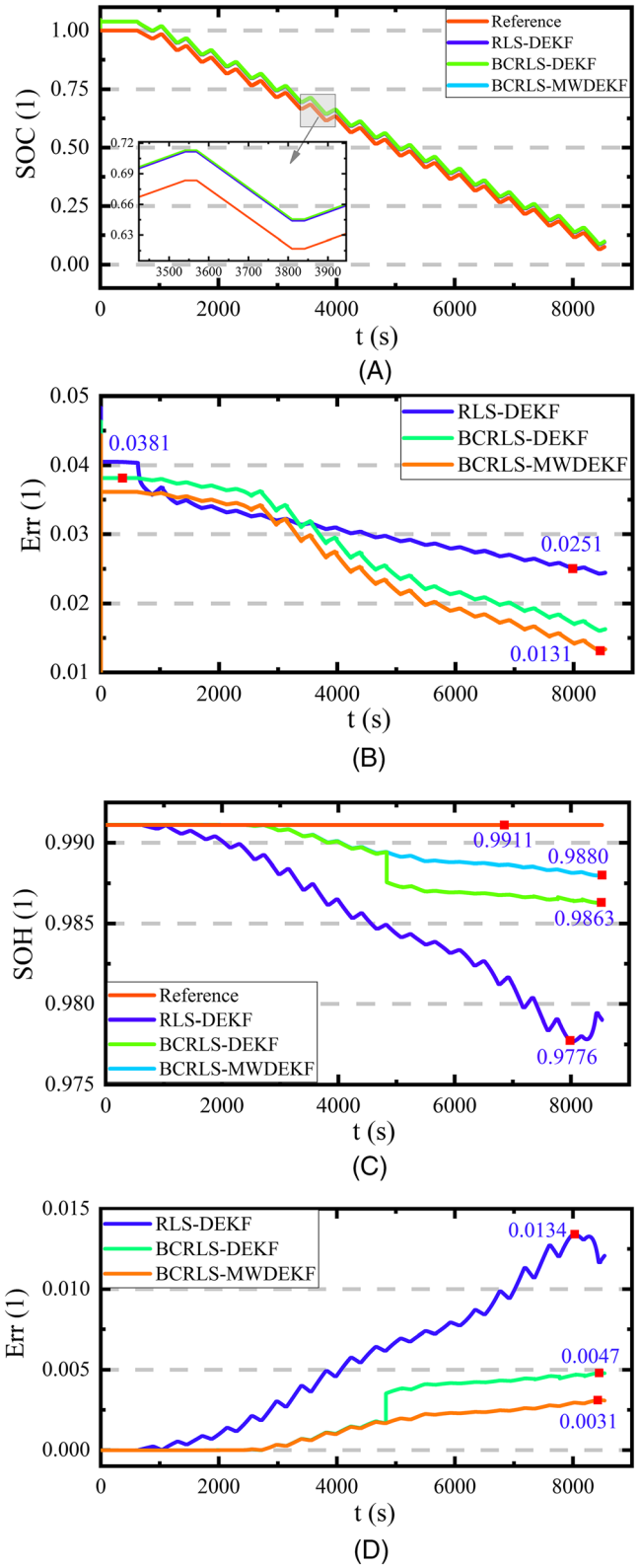

FIGURE 8 SOC and SOH co-estimation results under DST operating condition. (A) Comparison between estimated and reference SOC. (B) SOC estimation error. (C) Comparison between estimated and reference SOH. (D) SOH estimation error.

TABLE 1 Comparison of SOC and SOH co-estimation results of different algorithms under DST working condition.

Estimation method	RLS-DEKF	BCRLS-DEKF	BCRLS-MWDEKF
SOC maximum error	4.05%	3.81%	3.61%
SOC MAE	3.08%	2.80%	2.58%
SOC RMSE	3.11%	2.91%	2.70%
SOH maximum error	1.34%	0.47%	0.31%
SOH MAE	0.54%	0.21%	0.13%
SOH RMSE	0.69%	0.28%	0.17%

TABLE 2 Comparison of SOC and SOH co-estimation results of different algorithms under BBDST working condition.

Estimation method	RLS-DEKF	BCRLS-DEKF	BCRLS-MWDEKF
SOC maximum error	3.17%	4.21%	2.82%
SOC MAE	2.09%	1.55%	1.30%
SOC RMSE	2.49%	1.82%	1.62%
SOH maximum error	2.69%	2.28%	1.89%
SOH MAE	1.22%	0.80%	0.59%
SOH RMSE	1.48%	1.06%	0.81%

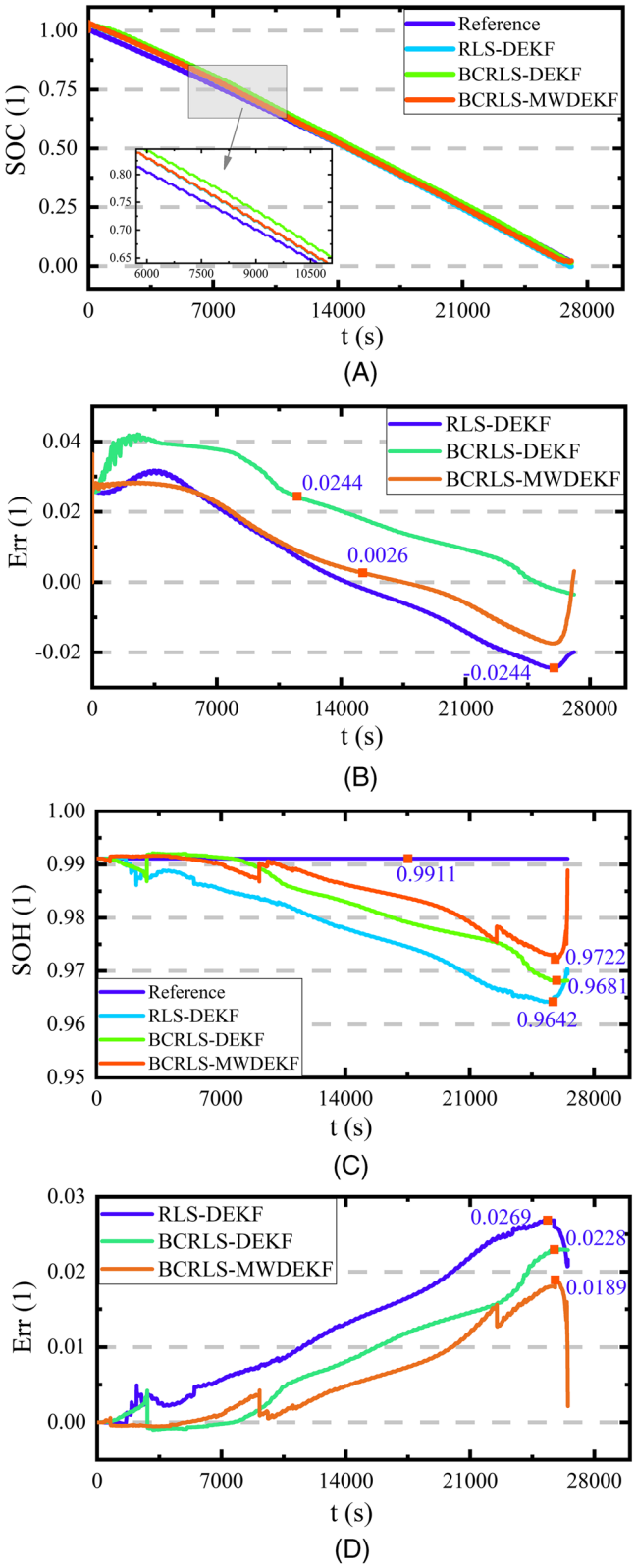

FIGURE 9 SOC and SOH co-estimation results under BBDST operating condition. (A) Comparison between estimated and reference SOC. (B) SOC estimation error. (C) Comparison between estimated and reference SOH. (D) SOH estimation error.